J Mater Sci: Mater Electron (2013) 24:5183–5188
DOI 10.1007/s10854-013-1542-2

Preparation and characterization of $Ni_{0.6}Mn_{2.4}O_4$ NTC ceramics by solid-state coordination reaction

Chengjian Ma · Yunfei Liu · Yinong Lu · Hong Gao · Hao Qian · Jianxiang Ding

Received: 14 August 2013 / Accepted: 8 October 2013 / Published online: 16 October 2013

Abstract The impact of synthesis parameters, such as calcination temperature and reaction time, on the microstructure, phase compositions and electrical properties of $Ni_{0.6}Mn_{2.4}O_4$ negative temperature coefficient (NTC) ceramics, which were synthesized via solid-state coordination reaction method, was systematically explained. With enhancing calcination temperature and time, the relative densities were raised, while the porosities diminished. A compact single-phase cubic spinel ceramic could be obtained after annealing at 1,100 and 1,150 °C, while a secondary phase Mn_3O_4 was detected when the annealing temperature raised to 1,200 °C. For the ceramics calcinated at 1,100 or 1,150 °C for 3 h, their resistivities were 2,133 and 2,178 Ω cm, the thermal constant B, which reflects the temperature sensitivity of the NTC ceramics, were 3,820 and 3,857 K. While the ceramic prepared at 1,200 °C for 3 h, the resistivity and the B value reached 2,273 Ω cm and 3,810 K, respectively. This phenomenon was attributed to the increase of lattice parameters and the reduction of Mn^{4+}–Mn^{3+} at high temperatures.

1 Introduction

Manganese-based transition-metal spinel oxide ceramics have been attracting substantial attentions as negative temperature coefficient (NTC) thermistors in various domestic and industrial applications due to their high temperature sensitivity, fast response, convenience in use, and low cost [1–3]. Diverse approaches were developed to prepare powders for NTC ceramics, such as the oxalate co-precipitation method [4, 5], the Pechini method [6], etc. The solid-state coordinate reaction method [7, 8] stands out from those methods because of some unique advantages, such as non-pollution, the accurate stoichiometry, etc.

To full fill the requirement of suitable resistivity, B value and high stability, many ions were doped into the nickel manganite NTC ceramics [9, 10]. However, the effects of sintering temperature [11, 12], rate of cooling, duration of sintering and milling time [13] on the final performances of NTC ceramics were extremely significant. It was found that the electrical resistivity of the slow cooled $Ni_{0.75}Mn_{2.25}O_4$ ceramic was 4,220 Ω cm, while the resistivity was only 3,197 Ω cm for the quenched sample [6]. Justin M. Varghese [14] reported that the resistivity of Ni–Mn–Fe–Cr–O ceramic, fabricated via traditional solid-state method, increased with the increasing of sintering temperature, and the decomposition of cubic spinel occurred when the sintering temperature was above 1,200 °C. The resistivities of $Ni_{2-x}Mn_xCo_{1.0}O_4$ and $Ni_{1.0}Mn_{1.0}Co_{1-x}Fe_xO_4$ thick films decreased and then increased with the increasing of sintering temperature [15]. So far, it is barely reported about the influence of sintering temperature on microstructure, phase composition and electrical property of the un-doped $Ni_{0.6}Mn_{2.4}O_4$ ceramic.

The present study focuses on the synthesis of NTC ceramics by solid-state coordination reaction and the effects of calcination temperature, sintering temperature and soaking time on the relative density, lattice parameter, porosity, grain size, DC electrical resistivity and thermistor constant have been systematically investigated.

C. Ma · Y. Liu (✉) · Y. Lu (✉) · H. Gao · H. Qian · J. Ding
State Key Laboratory of Materials-Oriented Chemical Engineering, College of Materials Science and Engineering, Nanjing University of Technology, Nanjing 210009, China
e-mail: yfliu@njut.edu.cn

Y. Lu
e-mail: yinonglu@njut.edu.cn

2 Experimental

2.1 Preparation of nickel manganese ceramics

Pure oxalate precursor $Ni_{0.6}Mn_{2.4}(C_2O_4)\cdot nH_2O$ was prepared by solid-state coordination reaction. Analytical reagent $Ni(CH_3COO)_2\cdot 4H_2O$, $Mn(CH_3COO)_2\cdot 4H_2O$, and $H_2C_2O_4\cdot 2H_2O$ were used as raw materials. A powder mixture with a molar ratio of 0.6:2.4:4.5 (Ni^{2+}:Mn^{2+}:oxalic acid) was ball milled for 5 h and then was dried at 80° for 24 h. The oxalate precursor was calcined at different temperatures for 4 h. Powders calcined at 700 °C were used to form disk-shaped samples. Subsequently, the samples were sintered at different temperatures from 1,000 to 1,200 °C for 3 and 5 h, and furnace-cooled to room temperature.

2.2 Characterization

The X-ray diffraction (XRD) patterns of the powder and the ceramics were recorded with a powder X-ray diffractometer (SmartLab, Rigaku, Japan). The microstructural features of the ceramics were analyzed using SEM (JSM-6510, JEOL Ltd., Japan). The bulk densities ρ_{bulk} of the ceramics were determined by the Archimedes method in water, and their relative density ρ_{rel} was calculated from the formula $\rho_{rel} = \rho_{bulk}/\rho_{th}$, where ρ_{th} is the theoretical density as obtained from XRD data of ceramics.

The resistances at 25° and 50 °C were measured with an Agilent 4294A precision impedance analyzer, during which the ceramics were immersed in a thermostat, whose temperature fluctuation around the designated value was ±0.1 °C. The $B_{25/50}$ value was calculated according to the formula $B_{25/50} = 3,850.16\ln(R_{25}/R_{50})$, where R_{25} and R_{50} were the resistances at 25 and 50 °C, respectively.

3 Results and discussion

The XRD pattern of the dried nickel-manganese oxalate precursor is given in Fig. 1. The XRD result shows that the as-prepared nickel-manganese oxalate precursor is a single phase $Ni_{0.6}Mn_{2.4}(C_2O_4)_3\cdot nH_2O$, apparently the same as the manganese oxalate (JCPDS 25-0544), and different from the nickel oxalate (JCPDS 25-0582). No characteristic peaks of the raw materials were detected in the dried precursor, which indicates that the reaction was completed.

Figure 2 illustrates the XRD patterns of the nickel–manganese oxide powder obtained by calcining precursor for 4 h at different temperatures. The results show that $Ni_{0.6}Mn_{2.4}O_4$ spinel is formed at 400°. Broadening of the peaks indicates that the powder is not well crystallized and the grain size is small. Cubic spinel structure $(Ni–Mn)_3O_4$ (JCPDS 84-0542) and tetragonal spinel structure Mn_3O_4 (JCPDS 18-0803) coexist when the precursor is calcined at 500° and 600 °C, which are the same as J.L. Martin de Vidales's [16] and T. Yokoyama's [17] results. While the calcination temperature

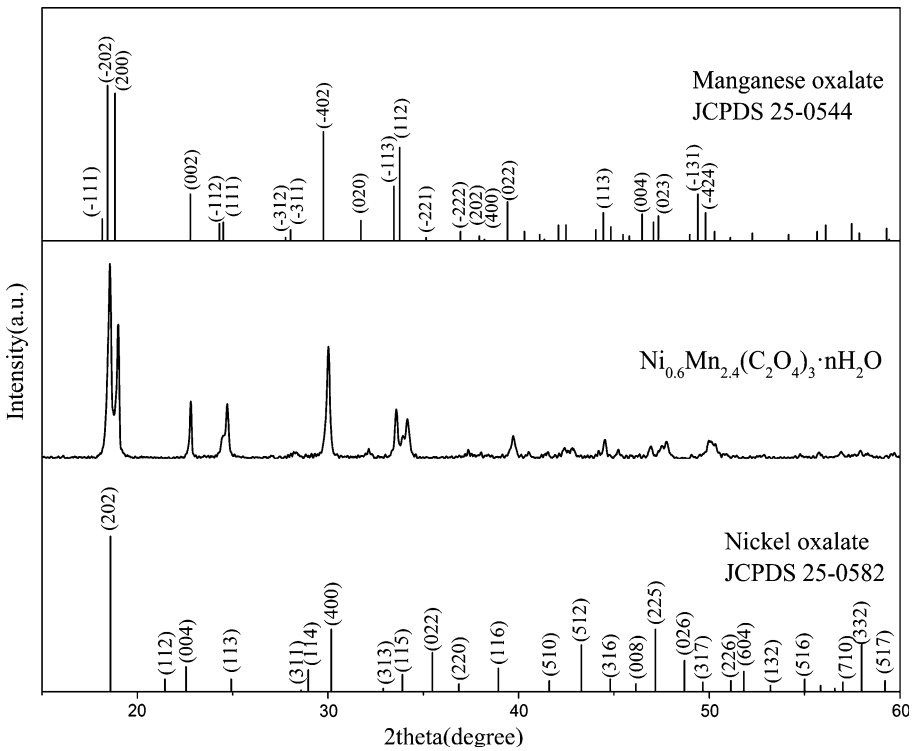

Fig. 1 XRD pattern of the oxalate $Ni_{0.6}Mn_{2.4}(C_2O_4)_3\cdot nH_2O$ prepared by solid-state coordination reaction. The standard patterns of $MnC_2O_4\cdot 2H_2O$ (JCPDS 25-0544) and $NiC_2O_4\cdot 2H_2O$ (JCPDS 25-0582) are also presented at the *top* and *bottom* for comparison, respectively

raises above 700 °C, the tetragonal spinel Mn_3O_4 disappears, a single cubic spinel $Ni_{0.6}Mn_{2.4}O_4$ powder is obtained.

Figure 3 illustrates the XRD patterns of the ceramics sintered at different temperatures for 5 h. When the sintering temperature is below 1,150 °C, a single cubic phase spinel structure can be obtained. Secondary phase, Mn_3O_4 (Hausmannite) with tetragonal structure, is detected when the ceramic sintered at 1,200 °C, and the peaks are broaden, which was also reported by K. Park [12]. We believe that the $Ni_{0.6}Mn_{2.4}O_4$ is decomposed partially to small grains, which leads to the broadening of (311) spinel reflection. For $Ni_{0.6}Mn_{2.4}O_4$, the decomposition would occur at 1,200 °C by the formula (1),

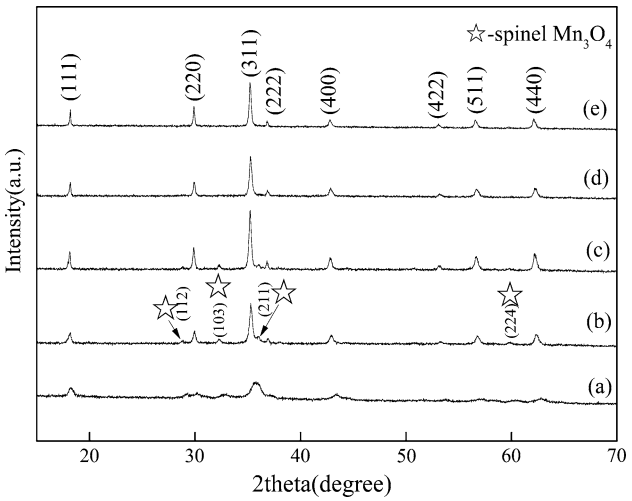

Fig. 2 XRD patterns of the nickel-manganese oxide powder obtained by calcining precursor for 4 h at different temperatures. (*a*) 400 °C, (*b*) 500 °C, (*c*) 600 °C, (*d*) 700 °C, (*e*) 800 °C

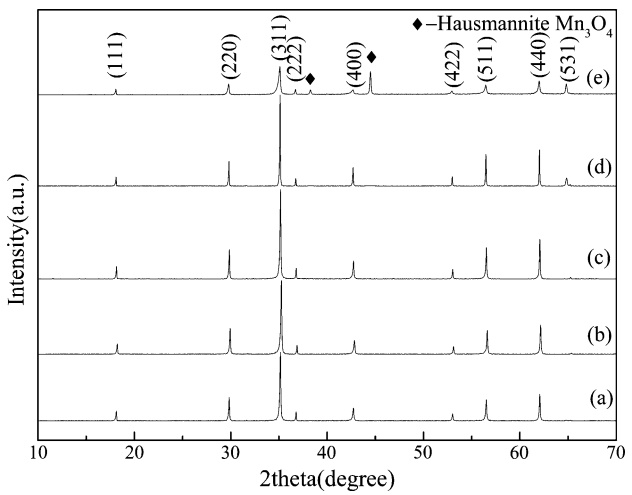

Fig. 3 XRD patterns of the ceramics sintered at different temperatures for 5 h. (*a*) 1,000 °C, (*b*) 1,050 °C, (*c*) 1,100 °C, (*d*) 1,150 °C, (*e*) 1,200 °C

$$Ni_{0.6}Mn_{2.4}O_4 \rightarrow xMn_3O_4 - 4x/3O_2 + (3-x)/3Ni_{1.8/(3-x)}Mn_{(7.2-9x)/(3-x)}O_4 \quad (1)$$

In addition, it is found that the diffraction peaks shift slightly to the low-angle direction, which indicates the lattice constant increases when the sintering temperature raised from 1,000 to 1,200 °C. This phenomenon can be caused by oxidation–reduction reactions and cation migrations within or between sublattices of the spinel structure [18, 19], expressed by formula (2),

$$Mn_A^{2+} + Mn_B^{4+} + Ni_B^{2+} \rightarrow 2Mn_B^{3+} + Ni_A^{2+}. \quad (2)$$

The lattice constant of the spinel is controlled by the cation-oxygen distances, which vary depending on the valence and coordination of the cations. Based on the data presented by Castelan [20] and Fang Daolai [21], the cation-oxygen distances are Mn_B^{4+}–$O = 1.843$ Å, Mn_B^{3+}–$O = 2.045$ Å, Mn_A^{2+}–$O = 2.041$ Å, Ni_B^{2+}–$O = 2.088$ Å, Ni_A^{2+}–$O = 1.97$ Å. According to formula (2), the increase in lattice constant observed in the present experiment could well indicates that a fraction of Mn^{4+} is reduced to Mn^{3+}.

Microstructure morphology of the sintered ceramics varies depending on the sintering temperature. SEM images of the ceramics sintered from 1,000 °C to 1,200° for 3 h are shown in Fig. 4. When the sintering temperature increasing, the pores content in the ceramics decreases. The grain size increases significantly from 2 to 9 μm with the increasing of sintering temperature. Dense structure can be obtained while the sintering temperature is higher than 1,100 °C. The ceramics prepared by solid-state coordinate reaction method has lower sintering temperature than that of the ceramics prepared by traditional solid-state method [14]. While the ceramics sintered at 1,200 °C, it is found that a number of small grains appear on the surface of the big grains. The decomposed regions are marked with ellipses in Fig. 4e. Therefore, the SEM results are well in agreement with that of XRD.

The relative densities of the ceramics sintered at different conditions are shown in Fig. 5. It is obvious that the relative density increases rapidly from 82.4 to 96.8 %, and then increases slightly to 97.8 % when the sintering temperature increases from 1,000 to 1,200 °C. Meanwhile, the density increases with the increasing of soaking time. Dense ceramics can be obtained when the sintering temperature is equal or higher than 1,100 °C.

The variations of electrical resistivities of the $Ni_{0.6}Mn_{2.4}O_4$ ceramics as a function of sintering temperature are shown in Fig. 6. For the ceramics sintered for 3 h, the room-temperature resistivity decreased rapidly from 4,327 to 2,133 Ω cm when the sintering temperature increased from 1,000 to 1,100 °C, and then increased slightly from 2,133 to 2,273 Ω cm when the sintering temperature further increased to 1,200 °C. Likewise, for

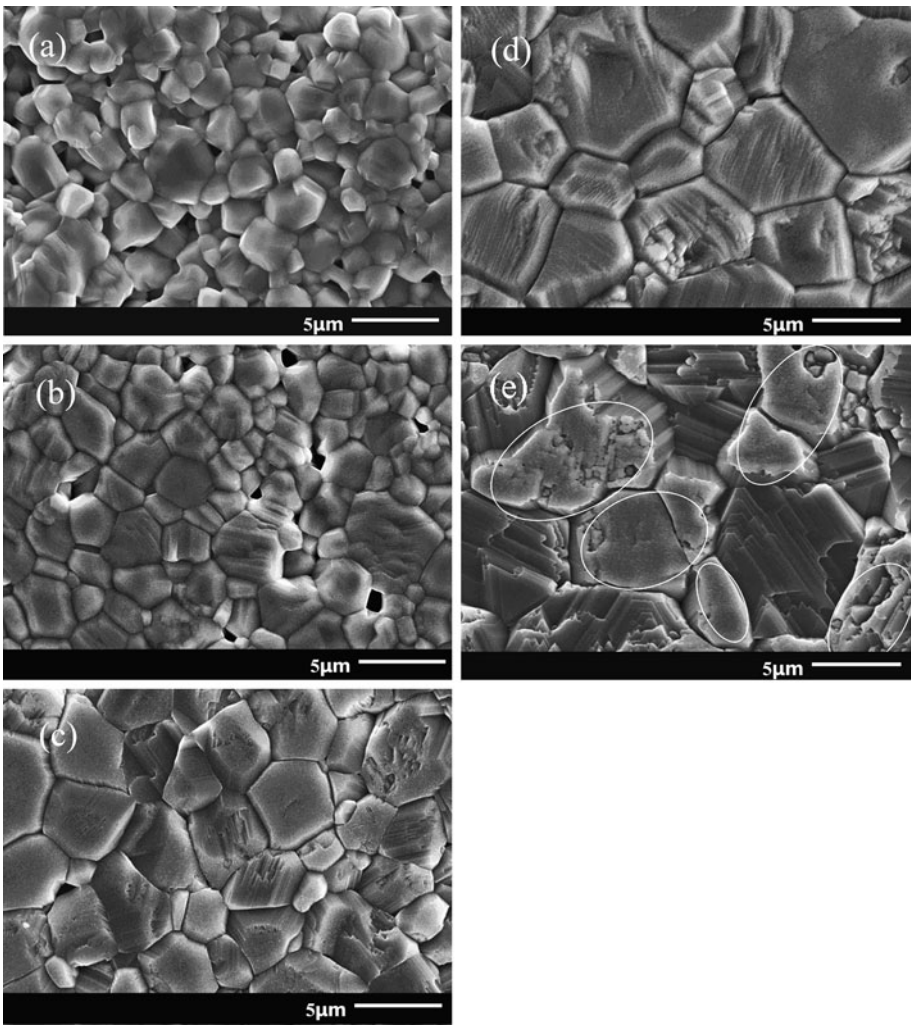

Fig. 4 SEM images of ceramics sintered at different temperatures for 3 h. **a** 1,000 °C, **b** 1,050 °C, **c** 1,100 °C, **d** 1,150 °C, and **e** 1,200 °C

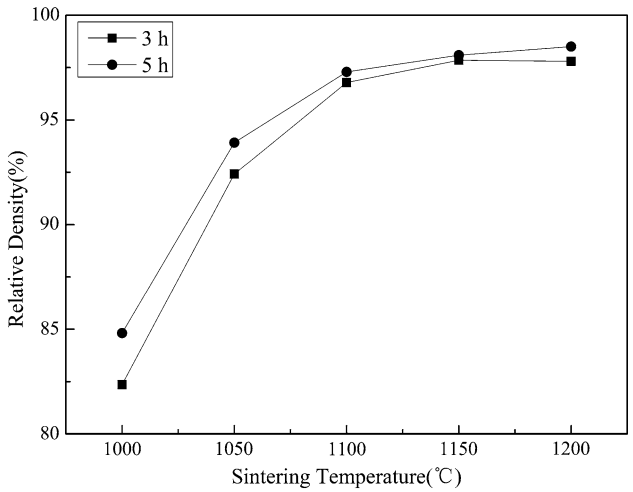

Fig. 5 Relative densities of $Ni_{0.6}Mn_{2.4}O_4$ ceramics sintered at different temperatures

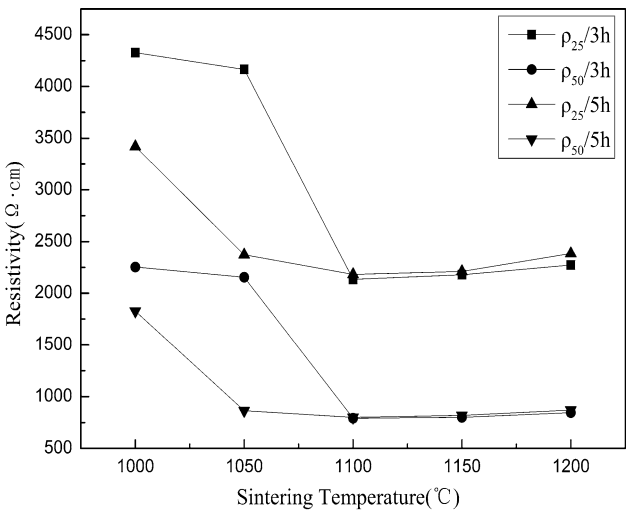

Fig. 6 The variations of electrical risistivities of the $Ni_{0.6}Mn_{2.4}O_4$ ceramics as a function of sintering temperature

the ceramics sintered for 5 h, the room-temperature resistivity decreased from 3,420 to 2,182 Ω cm, and then increased to 2,384 Ω cm. The resistivities decreased significantly when the test temperature increased from 25 to 50 °C.

Figure 7 shows the relationship between B value and sintering temperature. For the ceramics sintered for 3 h, when the sintering temperature increased from 1,000 to 1,200 °C, the B value increased from 2,513 to 3,857 K, and then decreased to 3,810 K. For the ceramics sintered for 5 h, the B value increased from 2,413 to 3,890 K when the sintering temperature increased from 1,000 to 1050 °C, and then decreased to 3,820 K when the sintering temperature increased to 1,200 °C. It is clear that the B value increased rapidly with increasing sintering temperature, indicating that the ceramic sensitivity improved. For practical applications, a higher value of the B is desirable because the resistivity is more sensitive to variation of temperature, providing more accurate and smaller variations in temperature measurements [22].

In the spinel, oxygen anions are cubic close packed and cations are situated at the tetrahedral sites and octahedral sites, the electrical conductivity is satisfactorily described by a phonon assisted hopping of charge carriers between Mn^{3+} and Mn^{4+} on octahedral sites of spinel structure induced by lattice vibrations.

During the study, we believe that the chemical composition of all $Ni_{0.6}Mn_{2.4}O_4$ ceramics are the same, so their physical properties depend mainly on the density, grain size, phase composition and cationic effect of its crystal sublattice. As previously reported [5], the total resistance is consist of bulk resistance, grain boundary resistance and electrode resistance. Factors affecting the resistivity can be explained as follows.

(1) When the grain size is less than a critical value, which is 9 μm in the research [23], the electrical resistivity

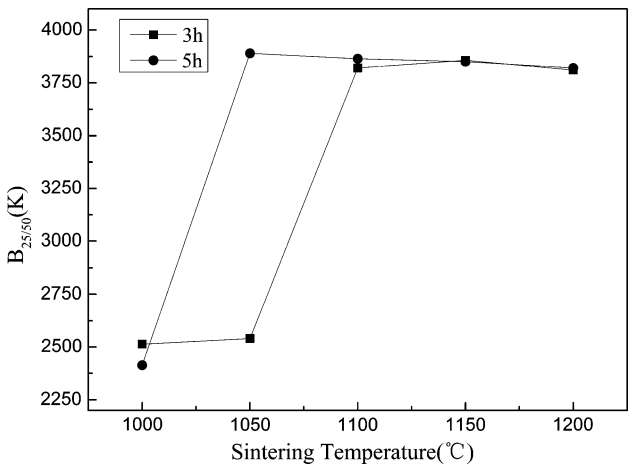

Fig. 7 The B-values with different sintering temperatures and soaking time in $Ni_{0.6}Mn_{2.4}O_4$ ceramics

decreases significantly with the increasing of grain size. The increase of grain size can reduce the grain boundary barrier, so the time and hoping probability among electron scattering events of charge carriers increase [12, 22, 24], as a result, the grain boundary resistivity decreases. (2) When sintered at low-temperatures, the ceramics can be regarded as the spinel-structured nickel manganite in composite of pores. With the increasing of density, the pores content reduces. Consequently, the resistivity decreases [25]. (3) When the sintering temperature raises from 1,000 to 1,200 °C, the notable increase of lattice parameter makes the hopping distance of charge carriers between Mn^{4+} and Mn^{3+} longer [26], thus the hopping of carriers is more difficult, resulting in the increase of the activation energy E_a, which helps the increase of the resistivity. (4) The con£uration of the Mn^{3+} and Mn^{4+} in octahedral position also governs the conductivity [27]. Indeed, in order to participate in hopping, the Mn^{3+} ions need to have in their vicinity of Mn^{4+} ion. Therefore, the ordering between Mn^{3+} and Mn^{4+} may disrupt the conduction. Due to the occurrence of reduction reaction, parts of Mn^{4+} reduces to Mn^{3+}, which gives rise to a decrease in the number of the Mn^{3+}/Mn^{4+} couples on octahedral sites, which are responsible for hopping and conductivity [24], resulting in an increase in resistivity.

When the sintering temperature is bellow 1,100 °C, the factors (1) and (2) resulting in the rapidly decrease of resistivity. However, while the sintering temperature is higher than 1,100 °C, the grain size and the density remain basically unchanged, the factors (3) and (4) dominate the change of the resistivity. Therefore, the resistivity increases slightly. These results indicate that the electrical properties of the NTC ceramics can be adjusted by changing sintering temperature.

When the ceramics were sintered at low temperatures, there are many pores in the ceramics, which have low negative temperature characteristic, resulting in the low B value of the ceramics. However, when the dense ceramics were sintered at high temperatures, the pores have little influence on the B value, so the B value changes slightly.

4 Conclusions

The increase of sintering temperature and soaking time produce appreciable changes in the phase, structural and electrical properties. High density ceramics could be obtained when the sintering temperature was higher than 1,100 °C, and single spinel phase could be achieved when the sintering temperature was bellow 1,150 °C. The grain size and porosity increased systematically with the increasing of sintering temperature and soaking time. For the ceramics sintered for 3 h, the electrical resistivity

changed from 4,327 to 2,133 Ω cm, on the contrary, the $B_{25/50}$ value increased previously from 2,513 to 3,857 K and decreased to 3,810 K later. For the ceramics sintered for 5 h, the electrical resistivity varied from 3,420 to 2182 Ω cm and then increased to 2,384 Ω cm, the $B_{25/50}$ value increased from 2,413 to 3,890 K, and then decreased to 3,820 K. In summary, the resistivities and the B values of the ceramics can be tuned by controlling the sintering process.

Acknowledgments This work is funded by the Priority Academic Program Development of Jiangsu Higher Education Institutions (PAPD) and the Program for Changjiang Scholars and Innovative Research Team in University (PCSIRT), IRT1146.

References

1. A. Feteira, J. Am. Ceram. Soc. **92**, 967–983 (2009)
2. W. Luo, H.M. Yao, P.H. Yang, C.S. Chen, J. Am. Ceram. Soc. **92**, 2682–2686 (2009)
3. A. Veres, J. Noudem, O. Perez, S. Fourrez, G. Bailleul, J. Eur. Ceram. Soc. **27**, 3873–3876 (2007)
4. S.A. Kanade, V. Puri, J. Alloy. Compd. **475**, 352–355 (2009)
5. H. Zhang, A. Chang, C. Peng, Microelectron. Eng. **88**, 2934–2940 (2011)
6. C. Zhao, Y. Zhao, Y. Wang, Solid State Commun. **152**, 593–595 (2012)
7. C.H. Zhao, B.Y. Wang, P.H. Yang, L. Winnubst, C.S. Chen, J. Eur. Ceram. Soc. **28**, 35–40 (2008)
8. D. Fang, Z. Wang, P. Yang, W. Liu, C. Chen, A.J.A. Winnubst, J. Am. Ceram. Soc. **89**, 230–235 (2006)
9. K. Park, S.J. Yun, J. Mater. Sci.: Mater. Electron. **15**, 359–362 (2004)
10. C. Peng, H. Zhang, A. Chang, F. Guan, B. Zhang, P. Zhao, J. Mater. Sci.: Mater. Electron. **23**, 851–857 (2012)
11. O.S. Aleksica, M.V. Nikolica, M.D. Lukovica, N. Nikolica, B.M. Radojcicb, M. Radovanovicc, Z. Djuricd, M. Mitrice, P.M. Nikolic, Mater. Sci. Eng. B. **178**, 202–210 (2013)
12. K. Park, J.K. Lee, J. Alloy. Compd. **475**, 513–517 (2009)
13. S. Liang, J. Yang, X. Yi, X. Zhang, Y. Bai, Ceram. Intern. **37**, 2537–2541 (2011)
14. J.M. Varghese, A. Seema, K.R. Dayas, J. Electroceram. **22**, 436–441 (2009)
15. K. Park, D.Y. Bang, J. Mater. Sci.: Mater. Electron. **14**, 81–87 (2003)
16. J.L. Martín de Vidales, R.M. Rojas, E. Vila, O. García-Martínez, Mater. Res. Bull. **29**, 1163–1173 (1994)
17. T. Yokoyama, T. Meguro, S. Okazaki, H. Fujikawa, T. Ishikawa, J. Tatami, T. Wakihara, K. Komeya, T. Sasamoto, Adv. Mater. Res. **29–30**, 359–362 (2007)
18. V.A.M. Brabers, J.C.J.M. Terhell, Phys. Stat. Sol. (a) **69**, 325–332 (1982)
19. D.A. Kukuruznyak, S.A. Bulkley, K.A. Omland, F.S. Ohuchi, M.C. Gregg, Thin Solid Films **385**, 89–95 (2001)
20. P. Castelan, B. Ai, I. Loubiere, A. Rousset, R. Legros, J. Appl. Phys. **72**, 4705–4709 (1992)
21. D. Fang, C. Chen, A.J.A. Winnubst, J. Alloy Compd. **454**, 286–291 (2008)
22. K. Park, I.H. Han, J. Electroceram. **17**, 1069–1073 (2006)
23. M. Hosseini, B. Yasaei, Ceram. Intern. **24**, 543–545 (1998)
24. K. Park, S.J. Kim, J.G. Kim, S. Nahm, J. Eur. Ceram. Soc. **27**, 2009–2016 (2007)
25. S.A. Kanade, Vijaya Puri. J. Alloy Compd. **475**, 352–355 (2009)
26. J.M. Varghese, A. Seema, K. Dayas, Mater. Sci. Eng. B. **149**, 47–52 (2008)
27. S.A. Kanade, V. Puri, Mater. Lett. **60**, 1428–1431 (2006)